J. Biochem. 129, 303–312 (2001)

Crystal Structure of Glucose Dehydrogenase from *Bacillus megaterium* IWG3 at 1.7 Å Resolution[1]

Keizo Yamamoto,*,[2] Genji Kurisu,† Masami Kusunoki,† Shiro Tabata,* Itaru Urabe,‡ and Shigeyoshi Osaki*

Department of Chemistry, Nara Medical University, Shijo, Kashihara, Nara 634-8521; †Institute for Protein Research, Osaka University, Suita, Osaka 565-0871; and ‡Department of Biotechnology, Graduate School of Engineering, Osaka University, Suita, Osaka 565-0871

Received October 16, 2000; accepted November 30, 2000

The crystal structure of glucose dehydrogenase (GlcDH) from *Bacillus megaterium* IWG3 has been determined to an *R*-factor of 17.9% at 1.7 Å resolution. The enzyme consists of four identical subunits, which are similar to those of other short-chain reductases/dehydrogenases (SDRs) in their overall folding and subunit architecture, although cofactor binding sites and subunit interactions differ. Whereas a pair of basic residues is well conserved among $NADP^+$-preferring SDRs, only Arg39 was found around the adenine ribose moiety of GlcDH. This suggests that one basic amino acid is enough to determine the coenzyme specificity. The four subunits are interrelated by three mutually perpendicular diad axes (P, Q, and R). While subunit interactions through the P-axis for GlcDH are not so different from those of the other SDRs, those through the Q-axis differ significantly. GlcDH was found to have weaker hydrophobic interactions in the Q-interface. Moreover, GlcDH lacks the salt bridge that stabilizes the subunit interaction in the Q-interface in the other SDRs. Hydrogen bonds between Q-axis related subunits are also less common than in the other SDRs. The GlcDH tetramer dissociates into inactive monomers at pH 9.0, which can be attributed mainly to the weakness of the Q-axis interface.

Key words: crystal structure, dissociation–association, glucose dehydrogenase, short-chain dehydrogenases/reductases, subunit interaction.

Glucose dehydrogenase (GlcDH; EC 1.1.1.47) catalyzes the oxidation of D-glucose to D-glucono-δ-lactone in the presence of coenzyme NAD^+ or $NADP^+$. $NAD(P)^+$ dependent GlcDH is produced by *Bacillus* species during endospore formation (*1–3*) and has been suggested to play a role in spore germination (*4–6*). The purified enzymes from *B. cereus* (*1*, *7*), *B. megaterium* M1286 (*2*), *B. megaterium* IAM1030 (*8*), and *B. subtilis* (*4*) have been characterized, and the GlcDH genes from *B. subtilis* (*9*) and from different strains of *B. megaterium*, M1286 (*10*), IWG3 (*11*), and IAM1030 (*12–14*), have been cloned and the corresponding expressed enzymes characterized. Amino acid sequence alignment revealed that GlcDHs from these *Bacillus* species have more than 80% homology (*14*).

Glucose dehydrogenase from *B. megaterium* is a tetrameric enzyme (M_r 112,800) with four identical subunits (*8*, *11*, *12*, *15*). GlcDH belongs to the family of short-chain dehydrogenases/reductases (SDRs) (*16*). More than 1,000 SDR DNA sequences have been registered in the sequence database (*17*), and more than 50 of these enzymes have been characterized (*16*). The active form of SDR enzymes is either a tetramer or a dimer, and each subunit typically consists of about 250 amino acid residues (*16*).

The three-dimensional structures of more than 10 members of the SDR family have been determined in the last decade (*18–37*). Despite their low sequence identities (no more than 30%), the three-dimensional structures of these enzymes show striking similarities in overall folding and intersubunit contacts. Accordingly, the overall structure of GlcDH is inferred to resemble those of the tetrameric SDRs of known structure. To date, however, only GlcDH shows a reversible dissociation-association of subunits under moderate conditions. The enzyme is inactivated in alkaline solution because of the dissociation of the tetramer into inactive monomers, which can reversibly associate into the fully active tetramer when the pH is lowered to 6.5 (*38–40*). The addition of 3 M NaCl prevents the alkaline dissociation, thereby stabilizing the tetramer structure (*39*).

To understand this remarkable feature that distinguishes GlcDH from other SDRs, information on the three-dimensional structure is indispensable. Here we report the

[1] This work was performed with the approval of the Photon Factory Program Advisory Committee (Proposal No. 97G078). This study was partly supported by grants from MESSC (G.K. and M.K.) and ACT-JST (M.K.). The coordinates have been deposited in the RSCB Protein Data Bank with accession code 1GCO.

[2] To whom correspondence should be addressed. Tel/Fax: +81-744-29-8810, E-mail: kama@naramed-u.ac.jp

Abbreviations: BphB, *Pseudomonas* sp. *cis*-biphenyl-2,3-dihydrodiol-2,3-dehydrogenase; DADH, *Drosophila lebanonensis* alcohol dehydrogenase; GlcDH, *Bacillus megaterium* glucose dehydrogense; 3α-HSDH, *Streptomyces hydrogenes* 3α,20β-hydroxysteroid dehydrogenase; 7α-HSDH, *Escherichia coli* 7α-hydroxysteroid dehydrogenase; 17β-HSDH, human estrogenic 17β-hydroxysteroid dehydrogenase; MLCR, mouse lung carbonyl reductase; SDR, short-chain dehydrogenase/reductase; THNR, *Magnaporthe grisea* trihydroxynaphthalene reductase; TR-II, *Datura stramonium* tropinone reductase II.

refined crystal structure of glucose dehydrogenase from *B. megaterium* IWG3 complexed with NAD^+ at 1.7 Å resolution, showing detailed subunit interactions and a comparison of the intersubunit interactions with those of other tetrameric SDR enzymes. The amino acid residues that determine coenzyme specificities are also discussed.

MATERIALS AND METHODS

Crystallization and Data Collection—Crystallization and data collection were described previously (*41*). Briefly, crystals of GlcDH in complex with NAD^+ were obtained by the hanging-drop vapor diffusion method with the micro-seeding technique (*42*) using PEG2000 as a precipitant. Rod-shaped crystals grew to a maximum size of 0.25 × 0.25 × 3.0 mm in 2 weeks.

A data set for structure analysis was collected on synchrotron radiation at the beamline BL-18B of the Photon Factory operated at 2.5 GeV at the High Energy Accelerator Research Organization, Japan. Reflections were recorded on 400 mm × 800 mm imaging plates mounted on a screenless Weissenberg camera for macromolecular crystals (*43*) with a cylindrical cassette of 430 mm radius at 290 K. The latent images were digitized on a Rigaku SOR-DS48 scanner. The X-ray images were processed and scaled with the programs DENZO and SCALEPACK (*44*).

Molecular Replacement—The crystal structure was solved by molecular replacement with the program AMoRe (*45*). Coordinates of 3α,20β-hydroxysteroid dehydrogenase (3α-HSDH, PDB code 2HSD) having 35.0% sequence identity with GlcDH was used as a search model. Since subunit architecture in the asymmetric unit, dimer or tetramer, was unknown for GlcDH, a dimer unit formed by chains A and C of 3α-HSDH was used. All amino acid residues except for glycine in 3α-HSDH were replaced by alanine for the calculation. Since the cross-rotation functions did not give a definite single solution, each of the six most probable solutions with higher correlation coefficients was subjected to subsequent translation function calculations. The solution giving the highest correlation coefficient of translation function was selected to further search for translational solution of a second dimer unit in repetition. Crystal packing was analyzed for each dimer using the program QUANTA (Molecular Simulations, Burlington MA, USA) to select the final four subunits. The best solution gave a correlation coefficient of 29.7% and an *R*-factor of 51.0% after rigid-body refinement using the program AMoRe. Two kinds of tetramers in the unit cell having different orientations were found as shown in Fig. 1.

Model Building and Structure Refinement—Structure refinement was carried out initially with the program XPLOR, version 3.84 (*46*), and at the later stages with the program CNS, version 0.9 (*47*). The model obtained by the molecular replacement calculation was used as the initial model. Improvement of the model was monitored with a free *R*-value calculated from 5% of randomly selected reflections, which were excluded from the refinement procedure. The asymmetric unit is represented by chains A, B, E, and F. In the initial stage of refinement, non-crystallographic symmetry restraints were applied separately between chains A and B and between chains E and F. Each chain pair belonged to the same tetramer. Alanine side chains of the model were replaced with the corresponding side chain of GlcDH in several steps during refinement, giving priority to regions of higher sequence identity in order to avoid model biases. Iterative refinement cycles by XPLOR were performed until the *R*-value dropped below 30% (R_{free} = 36.9%). Subsequently the molecular model was manually rebuilt in the maps with coefficients of sigma weighted $2F_o - F_c$ and $F_o - F_c$ maps using the program O, version 6.2.2 (*48*). The quality of the electron density map was improved significantly by the program DM (*45*) with solvent flattening, histogram matching and density modification options. At this refinement stage, non-crystallographic symmetry restraints were imposed on the four subunits in an asymmetric unit. NAD^+ molecules were incorporated into the model upon detection in $F_o - F_c$ difference maps. The crystallographic refinement was further continued with the program CNS after the resolution range of refinement was extended to 40–1.7 Å. In the final refinement stages, the residues from 39 to 55 were excluded from NCS restraints in consideration of the conformational differences among the chains resulting from crystal packing. After the first round of refinement (R = 22.0%, R_{free} = 22.8%), water molecules having peak heights above 3.0 σ in the $F_o - F_c$ maps and exhibiting acceptable hydrogen-bonding geometry were added to the model automatically using a water-pick option of CNS. Water molecules having *B*-values greater than 50 $Å^2$ were eliminated. The final *R*-value was 17.9% (R_{free} = 19.2%) for the resolution range of 40–1.7

TABLE I. **Data collection and refinement statistics of GlcDH.**

Data collection statistics	
Cell parameters: *a* (Å)	120.8 (1)
b (Å)	66.7 (1)
c (Å)	119.6 (1)
β (°)	93.25 (3)
Space group	*C*2
Total No. of reflections	357,354
No. of unique reflections	94,821
Completeness: % (range Å)	91.9 (100.0–1.70)
Outermost shell	77.3 (1.76–1.70)
R-merge[a]: % (range Å)	3.3 (100.0–1.70)
Outermost shell	16.6 (1.76–1.70)
$I/\sigma(I)$ (outermost shell)	29.2 (11.2)
Redundancy (outermost shell)	3.77 (3.71)
Radiation source	Photon Factory, Japan
Wavelength (Å)	1.0000
Refinement statistics	
Resolution range (Å)	40.0–1.70
R-factor (%)	17.9
Free *R*-factor (%)	19.2
Number of protein atoms	1972 × 4
Number of NAD^+ atoms	44 × 4
Number of solvent atoms	562
Rms deviations from ideal values	
Bond length (Å)	0.005
Bond angles (°)	1.2
Dihedrals (°)	21.9
Ramachandran plot statistics (%)	
Most favored residues	90.7
Allowed residues	9.3
Mean *B*-values ($Å^2$)	
All atoms	20.6
Main chain atoms	18.5
Side chain atoms	21.2
NAD^+ atoms	18.7
Solvent atoms	32.2

[a] $R_{merge} = \Sigma_{hkl}\Sigma_i|I(hkl)i - \langle I(hkl)\rangle|/\Sigma_{hkl} I(hkl)$, where $I(hkl)i$ is the *i*th measurement of the intensity of reflection *hkl* and $\langle I(hkl)\rangle$ is the mean intensity of reflection *hkl*.

Å. The stereochemistry of the model was verified using the software package PROCHECK (*49*). The refinement statistics are summarized in Table I.

RESULTS AND DISCUSSION

Quality of the Model—The crystal structure of GlcDH in complex with NAD^+ was determined by the molecular replacement method with chains A and C of 3α-HSDH as the search model. The model was refined to a crystallographic *R*-factor of 17.9% (R_{free} = 19.2%) for 94,821 unique reflections [$I_o > 2\sigma(I_o)$] in the resolution range of 40–1.7 Å. Table I summarizes the data collection and the results of the crystallographic refinement. A crystal asymmetric unit contains four chemically identical subunits (chains A, B, E, and F), four molecules of NAD^+, and 562 solvent molecules. The unit cell contains tetramers 1 and 2 (Fig. 1) comprising chains A, B, C, and D and chains E, F, G, and H, respectively. Tetramer 2 can be rotated around the R-axis by 84° into the same orientation as that of tetramer 1. The peptide chains were well defined in $2F_o - F_c$ maps. The pairwise rms discrepancies of the main chain atoms Cα, C, N, and O among the four crystallographically independent subunits vary at a value of 0.18 Å for pair A and B and 0.37 Å for pair A and E. The largest pairwise discrepancy along the chains was commonly observed at Lys41 located in the sur-

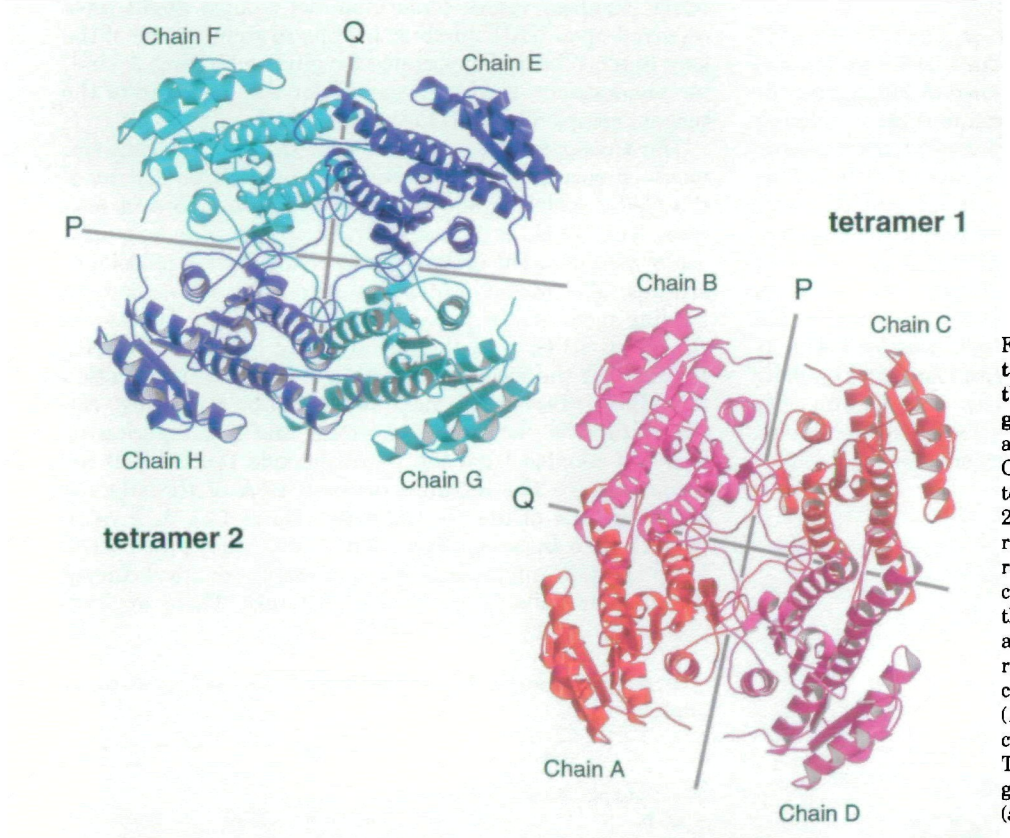

Fig. 1. **Ribbon representation of two tetramers of GlcDH viewed along the R-axes coinciding with crystallographic 2-fold axes.** Chains A, B, E, and F constitute the asymmetric unit. Chains C and D of tetramer 1 are related to chains A and B by the crystallographic 2-fold axis intersecting the center of tetramer 1. Similarly, chains G and H are related to chains E and F by another crystallographic 2-fold axis intersecting the center of tetramer 2. The three mutually perpendicular 2-fold axes in the tetrameric dehydrogenase molecules are conventionally designated as P, Q, and R (*18*). The R-axis of each tetramer coincides with a crystallographic 2-fold axis. The figure was produced with the programs MOLSCRIPT (*55*) and Raster3D (*57*).

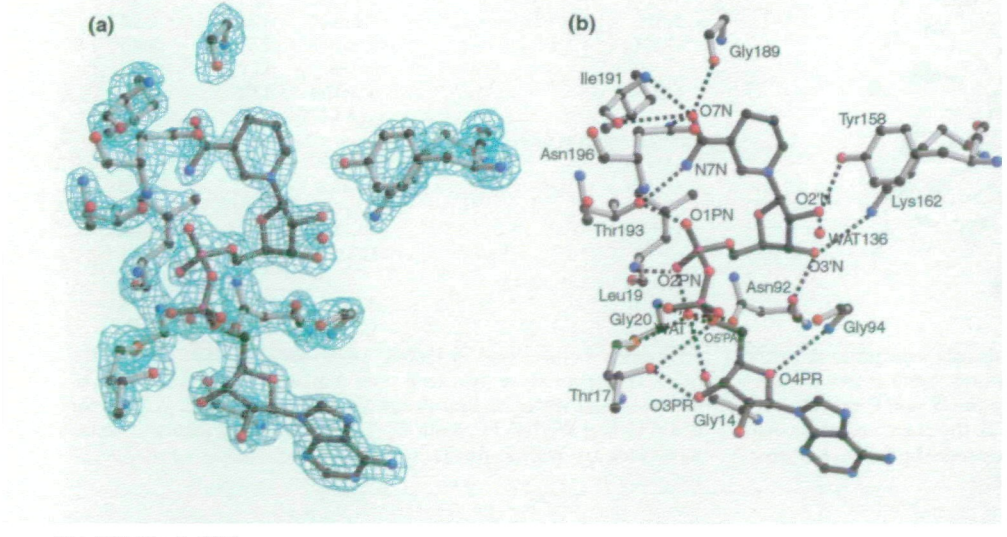

Fig. 2. **Mode of NAD^+ binding to the active site of GlcDH.** (a) Omit electron density map of ($F_o - F_c$) contoured at 4σ at a resolution range of 8.0 to 1.7 Å superimposed on models of NAD^+ and surrounding residues. (b) Possible hydrogen bonds between NAD^+ and protein. Hydrogen bonds are represented by broken lines. Oxygen, nitrogen and carbon atoms are colored red, blue and black, respectively. Bonds in protein and NAD^+ are colored white and gray, respectively. Both drawings were produced with the programs BOBSCRIPT (*56*) and Raster3D (*57*).

face loop (Arg39–Asp43) between βB and αC, where secondary structure is described in the next section. Located at a contact region of crystal packing is Lys41 of chain A rendering a weak salt bridge with Asp108 of chain D in the neighboring tetramer. The loop region formed at residues Arg39 to Asp43 is flexible, as reflected in the higher *B* values by about 10 Å^2 than the average value of all residues, thereby making the conformation of the loop susceptible to crystal packing influence. Differences in conformation are mainly at residues Arg39 to Asp43 and at the N-terminal region of helix αC (Glu44–Lys53). The rms deviation among the four subunits of the main chain atoms excluding the segment from Arg39 to Lys53 was 0.039 Å. The conformation of these four crystallographically independent subunits is therefore essentially identical.

Subunit Structure—The subunit structure of GlcDH shares the typical fold of the short chain dehydrogenases/reductases of known structure. As shown in Fig. 3, the subunit of GlcDH folds into a single domain of the α/β doubly wound structure (*51*) consisting of seven-stranded central parallel β-sheet sandwiched by two arrays of three α-helices (αC, αB, and αG on one side and αD, αE, and αF on the other side). Secondary structure elements were assigned according to the convention described by Ghosh *et al.* (*18*) to allow easier comparison between GlcDH and the other SDR members of known structure. The two βαβαβ motifs, βA-αB-βB-αC-βC and βD-αE-βE-αF-βF, constitute the dinucleotide binding motif, the Rossmann fold (*52*). The motif βD-αE-βE-αF-βF-αG-βG, together with an adjoining loop from Asp255 to Gly261, is responsible for substrate binding and tetramer formation. A loop region from Asn192 to Ile218 including helices αFG1 and αFG2 in the present crystal structure is well defined in electron density maps. The loop region is stabilized by several hydrogen bonds between the protein and NAD$^+$ (see below), which are more numerous in GlcDH than in other SDRs except for *Datura stramonium* tropinone reductase II (TR-II) (*36*).

This loop region contributes to the binding of the substrate (*19*, *27–30*, *33*, *36*). In apo-form or in complex with the cofactor, the loop region of SDR enzymes is disordered, whereas those in the ternary (enzyme-cofactor-substrate) complex are fixed because the substrate binding induces conformational change and stabilization of the loops (*19*, *27–30*, *33*). In the case of GlcDH, however, the loop region containing αFG1 and αFG2 is already fixed in the protein-NAD$^+$ complex where conformational change might have occurred upon NAD$^+$ binding, leading to stabilization of the loop in a conformation suitable for glucose binding. A similar phenomenon is also suggested for the structure of the ternary complex of TR-II (*36*).

The Conformation of NAD$^+$ and Its Binding Environment—Figure 2a shows the well-defined electron density of the NAD$^+$ molecule and the surrounding amino acid residues. The NAD$^+$ is bound to the enzyme in an extended conformation at the carboxyl ends of the central parallel β-strands. The overall conformation of the NAD$^+$ and its binding mode to the Rossmann fold is similar to those of the other SDRs, with the adenine ring in the *anti* conformation and the nicotinamide ring in the *syn* conformation (*52*). Both ribose rings have ^{2}E(C2′-*endo*) puckering. Nomenclature for the coenzyme atoms and sugar puckering forms is adopted from the polynucleotide IUPAC-IUB description (*53*). The distance between C6A of the adenine ring and C2N of the nicotinamide ring is 14.1 Å, a value very close to those in other SDRs (*18*, *21*, *28*, *31*, *34*). The NAD$^+$-protein interactions are essentially identical among the four subunits in the asymmetric unit. There are also

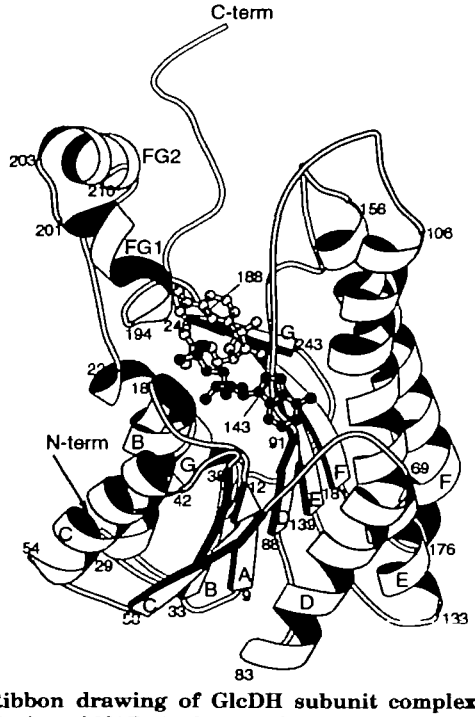

Fig. 3. **Ribbon drawing of GlcDH subunit complexed with NAD$^+$.** The bound NAD$^+$ is shown in ball-and-stick models. α-Helices B to G and β-strands A to G as well as the N and C termini are marked. The amino acid residues located at the start and end position of the α-helices and β-sheets are numbered. The figure was produced with the program MOLSCRIPT (*55*).

TABLE II. **Hydrogen bonds between NAD$^+$ and protein of GlcDH.**[a]

NAD$^+$	GlcDH		Mean distance[b] (Å)
Nicotinamide nucleoside moiety			
O7N	Asn196	ND2	3.15
	Gly189	O	3.34
	Ile191	N	2.85
	Ile191	O	3.45
N7N	Thr193	OG1	2.95
O3′N	Lys162	NZ	3.45
	Asn92	O	2.74
O2′N	Tyr158	OH	2.72
	WAT136	O[c]	2.77
Pyrophosphate moiety			
O1PN	Thr193	OG1	2.65
O2PN	Leu19	O	2.83
	WAT 1[d]		2.74
O5′PA	Thr17	OG1	3.56
	WAT 1[d]		2.94
Adenine ribose moiety			
O3PR	Thr17	OG1	2.65
O4PR	Gly94	N	3.54

[a]Hydrogen bonds were detected using the program CONTACT (*45*). [b]Distances were averaged over four subunits. [c]The functionally identical water molecules are WAT68 for chain B, WAT88 for chain C, and WAT65 for chain D. [d]The functionally identical water molecules are WAT36 for chain B, WAT12 for chain C, and WAT17 for chain D.

two well-ordered water molecules, which mediate hydrogen-bond interactions between NAD^+ and the interior surface of the protein. The interactions are shown in Fig. 2b and are summarized in Table II.

Nicotinamide Nucleoside Moiety—There are nine direct hydrogen bonds and one water-mediated hydrogen bond between the nicotinamide nucleoside moiety and the protein surface. The number of hydrogen bonds is greater in GlcDH than in other SDRs. Due to the close proximity of a loop region (residues 188–194) to the nicotinamide ring, additional interactions peculiar to GlcDH between this loop and the cofactor through hydrogen bonding may stabilize the loop region, which is essential for the formation of the active site cavity. A similar pattern of hydrogen bonding is found in TR-II (*36*). These interactions may allow the proper conformation of αFG1 and αFG2 for glucose binding.

Adenine Ring Moiety—No direct interactions are observed between the adenine ring and the internal surface of the protein. The adenine ring fits into a mostly hydrophobic pocket formed by Val66, Ala93 and the Cβ, Cγ, and Cδ atoms of Arg39. The plane of the Cβ, Cγ, and Cδ atoms is parallel to the adenine ring of NAD^+.

Adenine Ribose and Pyrophosphate Moiety—The adenine ribose and pyrophosphate moiety is situated on the turn between βA and αB (Gly14–Gly20), which is involved in the nucleotide-binding motif of the SDR members having the consensus sequence GXXXGXG (*16*). There are two hydrogen bonds between the protein and the adenine ribose and three hydrogen bonds between the protein and the

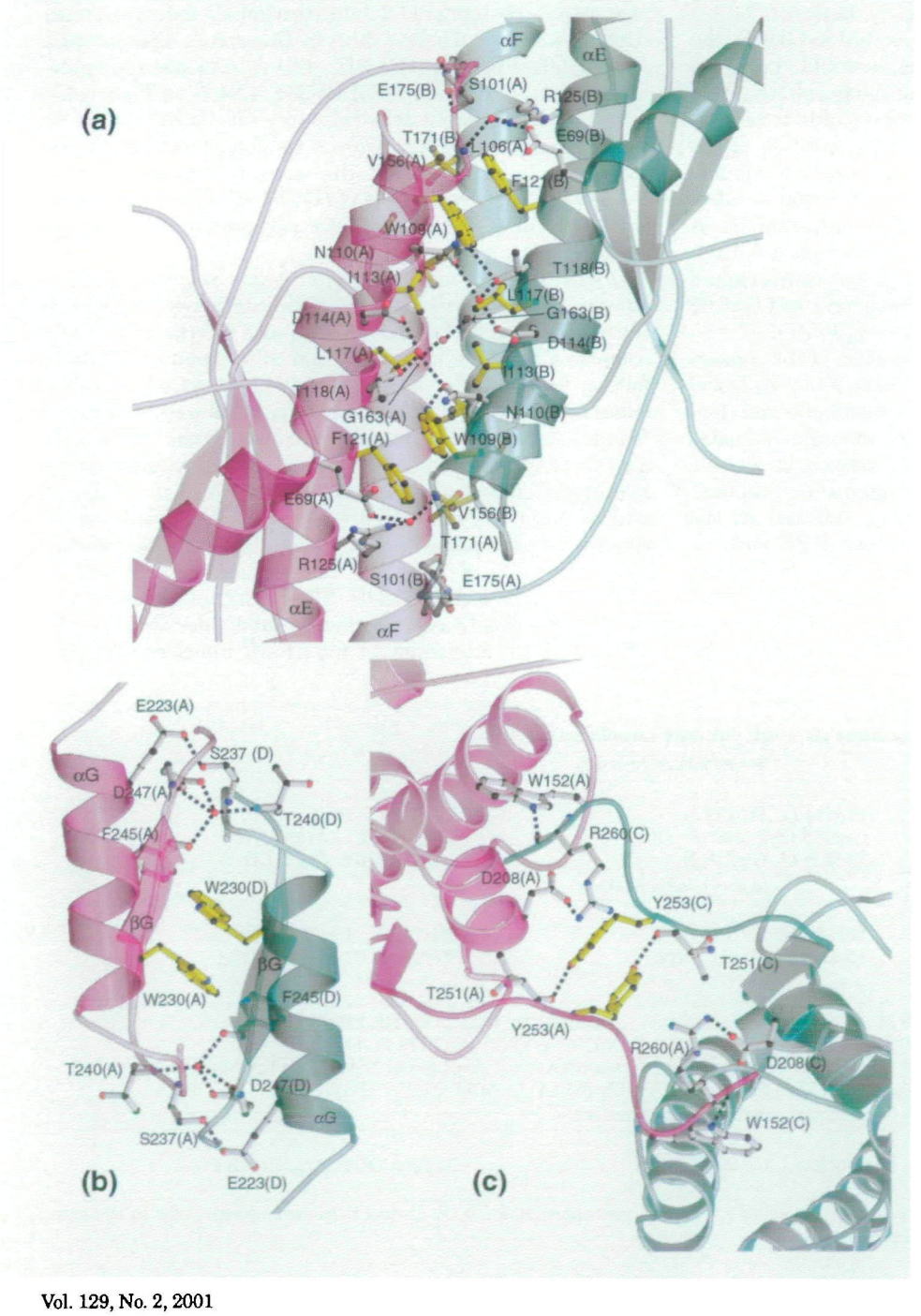

Fig. 4. **Major residues involved in non-covalent interactions at subunit interfaces.** The ribbon representations for Cα backbones are colored in magenta for chain A and in pale green for chains B, C, and D. Hydrophobic residues are shown in yellow, and other residues in white. Carbon, nitrogen, and oxygen atoms are colored black, blue and red, respectively. A, B, C, and D in parentheses after residue numbers refer to the chains A, B, C, and D where the residue is located. The probable hydrogen bonds are represented with broken lines. (a) Q-axis related interface. (b) P-axis related interface. (c) R-axis related interface.

pyrophosphate. Water-mediated hydrogen bonds are formed from the main chain Os of Gly14 and Thr17, the main chain NH of Gly20 and the OD1 of Asn92 to the O2'N and O5'PA of the NAD^+ as shown in Fig. 2b.

Coenzyme Specificity—GlcDH prefers $NADP^+$ to NAD^+ as the cofactor. The K_m value with $NADP^+$ as cofactor is about 10-fold lower than with NAD^+ (*54*). In most SDRs of known structure preferring NADP(H), two negative charges of the 2'-phosphate group are balanced by two positively charged residues (*27*, *29*, *35*, *36*). One of the basic residues is the conserved arginine residue located at the turn following the βB strand. In GlcDH, Arg39 is close to O2PR of the adenine ribose. The distance of 3.75 Å between CD of Arg39 and C6A of the adenine of GlcDH is very similar to the value of 3.74 Å for mouse lung carbonyl reductase (MLCR) (*29*). The distance between NH2 of Arg39 and O2PR of the adenine ribose of GlcDH is, however, 1.37 Å longer than that of MLCR. If $NADP^+$ bound to GlcDH, the conformation of the side chain of Arg39 would change to compensate for the negative charge of 2'-phosphate group of $NADP^+$. The other positively charged residue is usually Lys or Arg, which is located in the fourth position of the GXXXGXG consensus sequence of the dinucleotide binding motif of the SDR family (*29*, *35*, *36*) except for human estrogenic 17β-hydroxysteroid dehydrogenase (17β-HSDH). A basic residue is lacking in the 4th position of the GXXXGXG of 17β-HSDH, but instead the charge was compensated for by the interaction between the 2'-phosphate and Lys195 located in the flexible loop following strand βF (*27*).

Thr17 of GlcDH located in the 4th position of the consensus sequence forms a hydrogen bond with the 2'-hydroxyl group of the adenine ribose. The well-defined electron density around the adenine ribose moiety strongly indicates that no basic residues other than Arg39 compensate for the negative charges of the 2'-phosphate group. In addition, there is no ambiguous electron density detected in the main chain of the flexible loop region between βF and αG, which would provide a second basic residue to the 2'-phosphate group. These findings suggest that in GlcDH, only one basic residue is enough to compensate for the negative charges of the 2'-phosphate group and to determine the coenzyme specificity.

The Active Site Architecture—The active site of GlcDH consisting of the nicotinamide moiety of NAD^+ and the highly conserved Ser-Tyr-Lys catalytic triad (*16*), namely, Ser145, Tyr158 and Lys162, is very similar to that of the other SDR enzymes. The conserved tyrosine residue (Tyr-158) is considered as a general basic catalyst (*29*, *34*, *36*), and the pK_a value of its hydroxyl group is lowered by Lys162, leading to the stabilization of the tyrosinate anion at physiological pH (*29*, *34*, *36*).

The optimum pH of the oxidation reaction of GlcDH is 8.0 (*12*), whereas those of other SDR enzymes are greater than 8.5. The distance between Tyr158 OH and Lys162 NZ for GlcDH is 4.06 Å, the shortest among the SDRs of known structure. The distance between the two residues is 4.23 Å in 3α-HSDH, 4.28 Å in MLCR, 4.32 Å in *Pseudomonas* sp. *cis*-biphenyl-2,3-dihydrodiol-2,3-dehydrogenase (BphB), 4.32 Å in TR-II, 4.39 Å in *Drosophila lebanonensis* alcohol dehydrogenase (DADH), 4.54 Å in mouse sepiapterine reductase, 4.71 Å in 17β-HSDH, 4.84 Å in *Eschrichia coli* 7α-hydroxysteroid dehydrogenase (7α-HSDH) and 4.84 Å in *Mycobacterium tuberculosis* enoyl-acyl carrier protein reductase. It is likely that the shorter distance between Tyr158 OH and Lys162 NZ of GlcDH stabilizes the deprotonated form of Tyr158 at lower pH, thereby lowering its optimum pH.

Q-Axis Related Interface—The Q-axis related interface has the most extensive intersubunit interaction among the three axis related interfaces. The Q-axis interface of GlcDH comprises two long helices αE and αF of subunit A, which form a four-helix bundle together with those of helices of subunit B. Hereafter, the word "subunit" is used instead of "chain." A second residue pair related by the 2-fold axis always accompanies a residue pair of interaction such as hydrogen bonding or hydrophobicity between one subunit and its symmetry mate. Hence here we describe only one of the two residue pairs in this section. Hydrophobic interactions especially of aromatic residues are predominant at the Q-axis interface of GlcDH (Fig. 4a) without forming any salt bridges. The Q-axis interface is subdivided into the αE-αE and αF-αF interfaces. In the αE-αE interface (Fig. 4a),

TABLE III. **List of hydrogen bond interactions through subunit interfaces.**[a]

P-axis related interface		
Direct hydrogen bonds		
Leu114 O...Glu257 NE2,	Pro214 O...Pro178 N,	Tyr217 O...Tyr238 OH
Gly219 N...Tyr238 OH,	Glu223 OE2...Ser237 OG,	Glu235 OE1...Arg26 NH1[b]
Tyr238 O...Asp247 N,	Tyr238 O...Gly248 N,	Gln252 NE2...Gly241 O
Q-axis related interface		
Direct hydrogen bonds		
Ser101 OG...Glu175 OE1,	Ser101 N...Glu175 OE2,	His102 N...Tyr176 OH
His102 ND1...Tyr176 OH,	Met104 O...Arg125 NH1,	Trp109 NE1...Thr118 OG1
Trp152 N...Thr171 OG1,		
Water-mediated hydrogen bonds		
Glu170(A)[c] OE1...WAT41 O...Lys149(B) O,		Lys149(A) O...WAT58 O...Glu170(B) OE1
Ser100(A) OG...WAT59 O...Glu175(B) OE2,		Glu175(A) OE2...WAT178 O...Ser100(B) OG
Leu106(A) N...WAT93 O...[Glu69(B) OE1,Arg125(B) NH1],		[Glu69(A) OE1, Arg125 (A) NH1] ...WAT143 O...Leu106(B) N
Asn1110(A) OD1...WAT193 O...[Asp114(B) OD2, Thr118(B) OG1],		Gly163 (A) O...WAT169 O...Gly163(B) O
R-axis related interface		
Direct hydrogen bonds		
Trp152 NE1...Arg260 O,	Pro153 O...Gly259 N,	Asp208 OD1...Arg260 NH2[b]
Thr251 O...Tyr253 OH,		

[a]Hydrogen bonds were detected using the program CONTACT (*45*). [b]Ion pair interaction. [c]A, B, C, and D in parentheses refer to the subunit A, B, C, and D where the residue is located.

the side chains of Trp109 in subunit A is stacked on that of Phe121 of subunit B. The hydrophobic residue Ile113 (A) faces Leu117 (B). Hydrogen bond interactions are listed in Table III.

Figure 5 shows the amino acid sequence alignment of the αE and αF helices among SDRs. In the αE-αE interface, four hydrophobic residues colored red are clustered in the space, of which interactions are partaken by two or more aromatic residues (Fig. 6). The αE-helix of GlcDH kinks at Leu117 (Fig. 4a) and similar kinks are also observed in other SDR enzymes (Fig. 6). In a dimeric SDR of DADH, the kink at αE serves to optimize the subunit–subunit interactions for dimer formation (*33*), while the kinks of 7α-HSDH, MLCR, BphB, and THNR serve to optimize the separation between the two αEs, in which every second and/or third hydrophobic residue is an aromatic residue.

αE helix region

GlcDH	106	LSDWNKVIDTNLTGAFLGSREAIKYFVE	133
3α-HSDH	100	SVERFRKVVDINLTGVFIGMKTVIPAMKD	128
7α-HSDH	108	MADFRRAYELNVFSFFHLSQLVAPEMEKN	136
MLCR	97	KEAFDRSFSVNLRSVFQVSQMVARDMINR	125
BphB	104	LDAAFDEVFHINVKGYIHAVKACLPALVAS	133
THNR	123	PEEFDRVFTINTRGQFFVAREAYKH	152

αF helix region

GlcDH	156	VHYAASKGGMKLMTETLALEY	176
3α-HSDH	150	SSYGASKWGVRGLSKLAAVELGT	172
7α-HSDH	157	TSYASSKAAASHLVRNMAFDLG	178
MLCR	147	ITYSSTKGAMTMLTKAMAMEL	167
BphB	153	PLYTAAKHAIVGLVRELAFEL	173
THNR	176	AVYSGSKGAIETFARCMAIDMADK	199

Fig. 5. **Alignments of amino acid sequences of tetrameric SDR enzymes whose folds resemble that of GlcDH.** Amino acid residues involved in hydrophobic interaction are colored red and those involved in ion pair interactions are colored blue. (a) αE-αE contact region. (b) αF-αF contact region.

On the contrary, every second or third residue of GlcDH and 3α-HSDH is a small residue such as Ile, Leu, and Val, leading to less extensive hydrophobic interactions (Figs. 5 and 6). It is unlikely that the kinks of GlcDH and 3α-HSDH would contribute to the optimization of hydrophobic interactions at the regions.

The numbers of hydrogen bonds and salt bridges between the Q-axis related subunit pairs are summarized in Table IV. One pair of salt bridges further stabilizes the αE-αE interfaces of other SDRs (Fig. 6), whereas no salt bridge is observed in GlcDH. In addition, the total number of hydrogen bonds and salt bridges in GlcDH between the Q-axis related subunit pair is one of the smallest in the SDR family. The weakness of the αE-αE interface of GlcDH compared to other SDRs is attributable to less extensive hydrophobic interactions and the absence of ion pair interactions.

In contrast to the αE-αE interface, there are no large hydrophobic residues on the αF-αF interface. Instead, the small hydrophobic residues Val156, Ala159, Ala160, Leu167, and Thr171 of subunits A and B are found. Consequently, the two αF helices are situated closer to each other than those in the αE-αE interface. The amino acid sequence alignment of the αF-helices is shown in Fig. 5. In the case of GlcDH, the side chain of Met168, which does not face the inner side of the four-helical bundle, and Gly163 and Gly164 of GlcDH do not contribute to the hydrophobic interactions. There are also no direct hydrogen bonds at the αF-αF interface (Table IV). Thus, interactions at the αF-αF interface are also likely to be weaker in GlcDH than the other SDR enzymes.

P-Axis Related Interface—Interactions between the P-axis–related subunits are not extensive compared to those of the Q-axis. The P-axis interface consists of αG and βG of subunit A and those of symmetry-related subunit D (Fig. 4b). In the αG-αG interface, the indole ring of Trp230(A) is stacked on that of subinit D. No direct hydrogen bond interaction is found in the αG-αG and βG-βG interfaces, but hydrogen bonds are formed between other parts of the P-axis related subunits. Direct hydrogen bond interactions

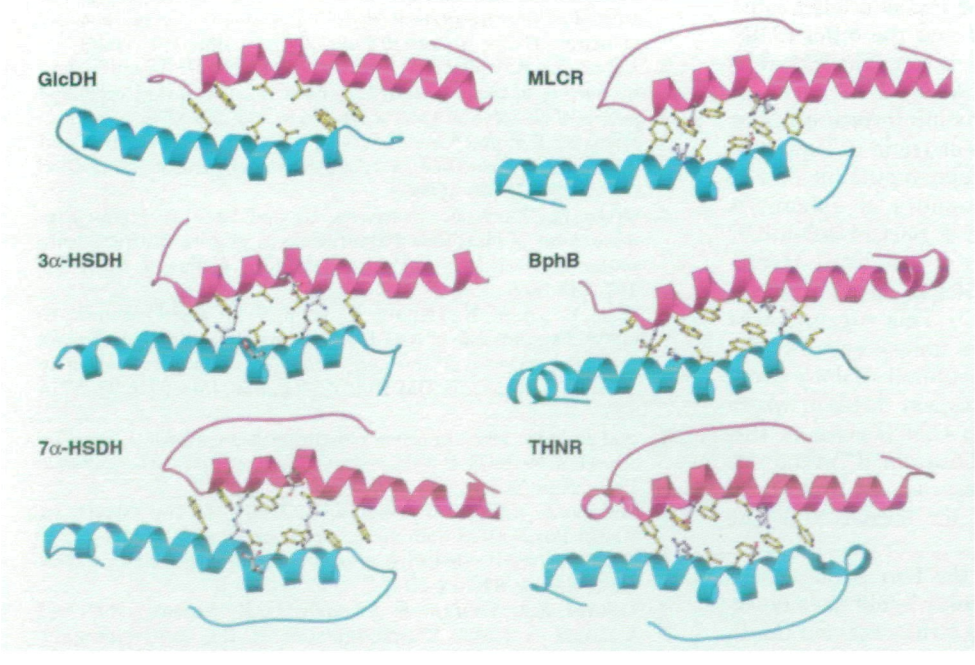

Fig. 6. **Comparison of subunit interactions at the αE-αE contact region of the Q-axis related interface.** Amino acid residues involved in hydrophobic interactions are colored yellow and those involved in ion pair interactions white. The figure was produced with the programs MOLSCRIPT (*55*) and Raster3D (*57*).

TABLE IV. **Comparison of the numbers of direct hydrogen bonds and salt bridges between Q-axis related subunits among SDR enzymes.**[a]

Enzyme	αE-αE contact		αF-αF contact		Total	
	Hydrogen bonds	Salt bridges	Hydrogen bonds	Salt bridges	Hydrogen bonds	Salt bridges
GlcDH	2	0	0	0	14	0
3α-HSDH	4	2	0	0	14	4
7α-HSDH	0	2	0	0	20	4
MLCR	0	2	0	0	12	2
BphB	4	2	2	0	22	4
THNR	6	2	2	0	20	2

[a]Hydrogen bonds and salt bridges were detected using the program CONTACT (*45*).

TABLE V. **Comparison of the numbers of direct hydrogen bonds and salt bridges between P-axis related subunits among SDR enzymes.**[a]

Enzyme	αG-αG contact		Other than αG-αG contact	
	Hydrogen bonds	Salt bridges	Hydrogen bonds	Salt bridges
GlcDH	0	0	16	2
3α-HSDH	0	0	28	2
7α-HSDH	0	0	24	0
MLCR	0	0	18	2
BphB	0	0	14	2
THNR	0	0	30	4

[a]Hydrogen bonds and salt bridges were detected using the program CONTACT (*45*).

and water-mediated hydrogen bonds are summarized in Table III. The interactions through the P-interface of GlcDH are weaker than those through the Q-interface. The tetrameric SDRs have no conserved amino acid residue or characteristic sequence motifs at the αG-helix region, ever though they have similar folds. Table V compares the direct hydrogen bonds for the P-axis related subunits among the SDRs. There are no direct hydrogen bonds at the αG-αG interface, whereas about 20 or more direct hydrogen bonds and salt bridges are observed between the P-axis related subunits. The buried solvent-accessible area around the P-axis interface of GlcDH is 1,600 Å^2 per subunit, which is similar to the mean value of 1,680 Å^2 per subunit of the other SDR members. Accordingly, the P-axis related interface is of similar strength in GlcDH and the other SDRs. The weakness of P-interface must be a common feature of SDRs of known structure (*18*, *23*, *28–30*, *32*).

R-Axis Related Interface—The R-axis interface contains only one prominent interaction: the side chain of Tyr253(A) is stacked on that of its symmetry-related subunit C (Fig. 4c). The C-terminal amino acid residues of subunit A [Phe255(A)–Gly261(A)] interact with a part of subunit C and are close to the active site cavity of subunit C. Hydrogen bonds are listed in Table III. GlcDH dissociates into inactive monomers at pH 9.0 (*38–40*). This suggests that the C-terminal region of subunit C is indispensable to the formation of the active site cavity of subunit A. Jany *et al.*, showed that GlcDH from *B. megaterium* M1286, which shows 82.8% sequence identity with GlcDH used in this study, is inactivated by chemical modification of Tyr253 (*10*, *15*). The result indicated the importance of C-terminal region of R-axis related subunit C for formation of the active site cavity of subunit A.

In the tetrameric SDR enzymes, the four subunits are related by three mutually perpendicular 2-fold axes designated as P, Q, and R. The quaternary structures and the P- and Q-axis interfaces are similar among the tetrameric SDRs. Some SDRs have a few direct interactions among the R-axis related subunits, while others such as 7α-HSDH (*28*) and THNR (*30*) have none at all. Hence, the tetrameric structures of SDR enzymes, as well as that of GlcDH, are mainly maintained by the interactions through the P- and Q-axis interfaces. Only GlcDH exhibits a remarkable feature of a reversible dissociation–association of subunits under moderate conditions (*38–40*). Comparison of the subunit interactions reveals that the interactions between the P-axis related subunits are similar among SDR enzymes and the interactions of the P-interface are weak compared to the Q-interface. Moreover, the interactions through the Q-axis related interface of GlcDH are weaker than those of other SDRs. The strength of the interactions of the Q-axis related interface, especially αE-αE contact, might be insufficient to maintain the tetrameric structure of GlcDH at pH 9.0.

We thank Drs N. Watanabe, M. Suzuki, and N, Igarashi for help with data collection at Photon Factory. We thank Dr. Elizabeth P. Ko-Mitamura for critical reading of the manuscript.

REFERENCES

1. Bach, J.A. and Sadoff, H.L. (1962) Aerobic sporulation bacteria. I. Glucose dehydrogenase of *Bacillus cereus*. *J. Bacteriol.* **83**, 699–707
2. Pauly, H.E. and Pfleiderer, G. (1975) D-Glucose dehydrogenase from *Bacillus megaterium* M 1286: purification, properties, and structure. *Hoppe-Seyler's Z. Physiol. Chem.* **356**, 1613–1623
3. Fujita, Y., Ramaley, R., and Freese, E. (1977) Location and properties of glucose dehydrogenase in sporulating cells and spores of *Bacillus subtilis*. *J. Bacteriol.* **132**, 282–293
4. Ramaley, R.F. and Vasantha, N. (1983) Glycerol protection and purification of *Bacillus subtilis* glucose dehydrogenase. *J. Biol. Chem.* **258**, 12558–12565
5. Otani, M., Ihara, N., Umezawa, C., and Sano, K. (1986) Predominance of gluconate formation from glucose during germination of *Bacillus megaterium* QM 1551 spores. *J. Bacteriol.* **167**, 148–152
6. Sano, K., Otani, N., Uehara, R., Kimura, M., and Umezawa, C. (1988) Primary role of NADH formed by glucose dehydrogenase in ATP provision at the early stage of spore germination in *Bacillus megaterium* QM B1551. *Microbiol. Immunol.* **32**, 877–885
7. Sadoff, H.L. (1966) Glucose rehydrogenase—soluble I. *Bacillus cereus* in *Methods in Enzymology* Vol. 9, pp. 103–107, Academic Press, New York
8. Makino, Y., Ding, J.-Y., Negoro, S., Urabe, I., and Okada, H. (1989) Purification and characterization of new glucose dehydrogenase from vegetative cells of *Bacillus megaterium*. *J. Ferment. Bioeng.* **67**, 372–379
9. Lampel, K.A., Uratani, B., Chuadhry, G.R., Ramaley, R.F., and Rudikoff, S. (1986) Characterization of the developmentally

regulated *Bacillus subtilis* glucose dehydroganase gene. *J. Bacteriol.* **166**, 238–243
10. Heilmann, H.J., Mägert, H.J., and Gassen, H.G. (1988) Identification and isolation of glucose dehydrogense genes of *Bacillus megaterium* M 1286 and their expression in *Escherichia coli*. *Eur. J. Biochem.* **174**, 485–490
11. Makino, Y., Negoro, S., Urabe, I., and Okada, H. (1989) Stability-incresing mutants of glucose dehydrogenase from *Bacillus megaterium* IWG3. *J. Biol. Chem.* **264**, 6381–6385
12. Mitamura, T., Urabe, I., and Okada, H. (1989) Enzymatic properties of isozymes and variants of glucose dehydrogenase from *Bacillus megaterium*. *Eur. J. Biochem.* **186**, 389–393
13. Mitamura, T., Evora, R.V., Nakai, T., Makino, Y., Negoro, S., Urabe, I., and Okada, H. (1990) Structure of isozyme genes of glucose dehydrogenase from *Bacillus megaterium* IAM1030. *J. Ferment. Bioeng.* **70**, 363–369
14. Nagao, T., Mitamura, T., Wang, X.H., Negoro, S., Yomo, T., Urabe, I., and Okada, H. (1992) Cloning, nucleotide sequences, and enzymatic properties of glucose dehydrogenase isozymes from *Bacillus megaterium* IAM1030. *J. Bacteriol.* **174**, 5013–5020
15. Jany, K.-D., Ulmer, W., Fröschle, M., and Phleiderer, G. (1984) Complete amino acid sequence of glucose dehydrogenase from *Bacillus megaterium*. *FEBS Lett.* **165**, 6–10
16. Jörnvall, H., Persson, B., Krook, M., Atrian, S., Gonzàlez-Duarte, R., Jeffery, J., and Ghosh, D. (1995) Short-chain dehydrogenase/reductases (SDR). *Biochemistry* **34**, 6003–6013
17. Jörnvall, H., Höög, J.-O., and Persson, B. (1999) SDR and MDR: completed genome sequences show these protein families to be large, of old origin, and of complex nature. *FEBS Lett.* **445**, 261–264
18. Ghosh, D., Weeks, C.M., Grouchulski, P., Duax, W.L., Erman, M., Rimsay, R.L., and Orr, J.C. (1991) Three-dimensional structure of holo 3α,20β-hydroxysteroid dehydrogenase: a member of a short-chain dehydrogenase family. *Proc. Natl. Acad. Sci. USA* **88**, 10064–10068
19. Ghosh, D., Wawrzak, Z., Weeks, C.M., Duax, W.L., and Erman, M. (1994) The refined three-dimensional structure of 3α,20β-hydroxysteroid dehydrogenase and possible roles of the residues conserved in short-chain dehydrogenases. *Structure* **2**, 629–640
20. Ghosh, D., Erman, M., Wawrzak, Z., Duax, W.L., and Pangborn, W. (1994) Mechanism of inhibition of 3α,20β-hydroxysteroid dehydrogenase by a licorice-derived steroidal inhibitor. *Structure* **2**, 973–980
21. Varughese, K.I., Skinner, M.M., Whiteley, J.M., Matthews, D.A., and Xhong, N.H. (1992) Crystal structure of rat liver dihydropreridine reductase. *Proc. Natl. Acad. Sci. USA* **89**, 6080–6084
22. Su, Y., Varughese, K.I., Xhong, N.H., Bray, T.L., Roche, D.J., and Whiteley, J.M. (1993) The crystallographic structure of a human dihydropreridine reductase NADH binary complex expressed in *Escherichia coli* by a cDNA constructed from its rat homologue. *J. Biol. Chem.* **268**, 26836–26841
23. Rafferty, J.B., Simon, J.W., Baldock, C., Artymiuk, P.J., Baker, P.J., Stuije, A.R., Slabas, A.R., and Rice, D.W. (1995) Common themes in redox chemistry emerge from the X-ray structure of oilseed rape (*Brassuca napus*) enoyl acyl carrier protein reductase. *Structure* **3**, 928–938
24. Ghosh, D., Pletnev, V., Zhu, D.-W., Wawrzak, Z., Duax, W.L., Pangborn, W., Labrie, F., and Lin, S.-X. (1995) Structure of human estrogenic 17β-hydroxysteroid dehydrogenase at 2.20 Å resolution. *Structure* **3**, 503–513
25. Azzi, A., Rehse, P.H., Zhu, D.-W., Campbell, R.L., Labrie, F., and Lin, S.-X. (1996) Crystal structure of human estrogenic 17β-hydroxysteroid dehydrogenase complexed with 17β-estradiol. *Nat. Struct. Biol.* **3**, 665–668
26. Breton, R., Housset, D., Mazza, C., and Fontecilla-Camps, J.C. (1996) The structure of a complex human 17β-hydroxysteroid dehydrogenase with estradiol and $NADP^+$ identifies two principal targets for the design of inhibitors. *Structure* **4**, 950–915
27. Mazza, C., Breton, R., Dominique, H., and Fontecilla-Camps, J.C. (1998) Unusual charge stabilization of $NADP^+$ in 17β-hydroxysteroid dehydrogenase. *J. Biol. Chem.* **273**, 8145–8152
28. Tanaka, N., Nonaka, T., Tanabe, T., Yoshomoto, T., Tsuru, D., and Mitsui, Y. (1996) Crystal structure of the binary and ternary complexes of 7α-hydroxysteroid dehydrogenase from *Escherichia coli*. *Biochemistry* **35**, 7715–7730
29. Tanaka, N., Nonaka, T., Nakanishi, M., Deyashiki, Y., Hara, A., and Mitsui, Y. (1996) Crystal structure of the ternary complex of mouse lung carbonyl reductase at 1.8 Å resolution: the structural origin of coenzyme specificity in the short-chain dehydrogenase/reductase family. *Structure* **15**, 33–45
30. Anderson, A., Jordan, D., Schneider, G., and Lindqvist, Y. (1997) Crystal structure of the ternary complex of 1,3,8-trihydroxysteroid naphthalene reductase from *Magnaporthe grisea* with NADPH and an active-site inhibitor. *Structure* **4**, 1161–1170
31. Auerbuch, G., Herrmann, A., Gütlich, M., Fischer, M., Jacob, U., Bacher, A., and Huber, R. (1997) The 1.25 Å crystal structure of sepiapterin reductase reveals its binding mode to pterins and brain neurotransmitters. *EMBO J.* **16**, 7219–7230
32. Hülsmeyer, M., Hecht, H.-J., Niefind, K., Hofer, B., Eltis, L.D., Timmis, K.N., and Schonburg, D. (1998) Crystal structure of *cis*-biphenyl-2,3-dihydrodiol-2,3-dehydrogenase from a PCB degrader at 2.0 Å resolution. *Protein Sci.* **7**, 1286–1293
33. Benach, J., Atrian, S., Gonzàlez-Duarte, R., and Ladenstein, R. (1998) The refined crystal structure of *Drosophila lebanonensis* alcohol dehydrogenase at 1.9 Å resolution. *J. Mol. Biol.* **282**, 383–399
34. Benach, J., Atrian, S., Gonzàlez-Duarte, R., and Ladenstein, R. (1999) The catalytic reaction and Inhibition mechanism of *Drosophila lebanonensis* alcohol dehydrogenase: observation of an enzyme-bound NAD-ketone adduct at 1.4 Å resolution by X-ray crystallography. *J. Mol. Biol.* **289**, 335–355
35. Nakajima, K., Yamashita, A., Akama, H., Natatsu, T., Kato, H., Hashimoto, T., Oda, J., and Yamada, Y. (1998) Crystal structure of two tropinone reductases: different reaction stereospecificities in the same protein fold. *Proc. Natl. Acad. Sci. USA* **95**, 4876–4881
36. Yamashita, A., Kato, H., Wakatsuki, S., Tomizaki, T., Nakatsu, T., Nakajima, K., Hashimoto, T., Yamada, Y., and Oda, J. (1999) Structure of tropinone reductase-II complexed with $NADP^+$ and pseudotropine at 1.9 Å resolution: implication substrate binding and catalysis. *Biochemistry* **38**, 7630–7637
37. Fisher, M., Kroon, J.T., Martindale, W., Stuitje, A.R., Slabas, A.R., and Rafferty, J.B. (2000) The X-ray structure of *Brassica napus* beta-keto acyl carrier protein reductase and its implications for substrate binding and catalysis. *Struct. Fold Des.* **4**, 339–347
38. Pauly, H.E. and Pfleiderer, G. (1977) Conformation and functional aspects of the reversible dissociation and denaturation of glucose dehydrogenase. *Biochemistry* **16**, 4599–4604
39. Maurer, E. and Pfleiderer, G. (1985) Reversible pH-induced dissociation of glucose dehydrogenase from *Bacillus megaterium* I. Conformational and functional changes. *Biochim. Biophys. Acta* **827**, 381–388
40. Maurer, E. and Pfleiderer, G. (1987) Reversible pH-induced association of glucose dehydrogenase from *Bacillus megaterium* II. Kinetics and mechanism. *Z. Naturforsch.* **42c**, 905–915
41. Yamamoto, K., kusunoki, M., Urabe, I., Tabata, S., and Osaki, S. (2000) Crystallization and preliminary X-ray analysis of glucose dehydrogenase from *Bacillus megaterium* IWG3. *Acta Crystallog. sect. D* **56**, 1443–1445
42. McPherson, A. (1982) *Preparation and Analysis of Protein Crystals*, 1st ed., pp. 96–97, John Wiley, New York
43. Sakabe, N. (1991) X-ray diffraction data collection system for modern protein crystallography with a Weissenberg camera and an imaging plate using synchrotron radiation. *Nucl. Instrum. Methods A* **303**, 448–463
44. Otwinowski, Z. and Minor, W. (1996) Processing of X-ray diffraction data collected in oscillation mode in *Methods in Enzymology*, Vol. 276, pp. 307–326, Academic Press, New York
45. Collaborative Computational Project Number 4 (1994) The CCP4 suite: programs for protein crystallography. *Acta Crystal-*

logr. sect D **50**, 760–763
46. Brünger, A.T. (1992) *XPLOR manual. version 3.1*, Yale University, New Haven
47. Brünger, A.T., Adams, P.D., Clore, G.M., DeLano, W.L., Gros, P., Grosse-Kunstleve, R.W., Jiang, J.-S., Kuszewski, J., Nilges, N., Pannu, N.S., Read, R.J., Rice, L.M., Simonson, T., and Warren, G.L. (1998) Crystallography and NMR system (CNS): A new software system for macromolecular structure determination. *Acta Crystallog. sect. D* **54**, 905–921
48. Jones, T.A., Zou, J.Y., Cowan, S.W., and Kjeldgaard, M. (1991) Improved methods for building protein models in electron density maps and the location of errors in the model. *Acta Crystallog. sect. A* **47**, 110–119
49. Laskowski, R.A., MacArthur, M.W., Moss, D.S., and Thornton, J.M. (1993) PROCHECK: a program to check the stereochemical quality of protein structures. *J. Appl. Crystallogr.* **5**, 802–810
50. Ramachandran, G.N., Ramakrishnan, C., and Sasisekharan, V. (1963) Stereochemistry of polypeptide chain configurations. *J. Mol. Biol.* **7**, 95–99
51. Orengo, C.A., Jones, D.T., and Thornton, J.M. (1994) Protein superfamilies and domain superfolds. *Nature* **372**, 631–634
52. Rossmann, M.G., Liljas, A., Branden, C.-I., and Banaszak, L.J. (1975) Evolutionary and structural relationships among dehydrogenases in *The Enzymes* (Boyer, P.D., ed.) 3rd. ed., Vol. 11A, pp. 61–102, Academic Press, New York
53. IUPAC-IUB Joint Commission on Biochemical Nomenclature (1983) Abbreviations and symbols for the description of conformations of polynucleotide chains. *Eur. J. Biochem.* **131**, 9–15
54. Nagao, T., Makino, Y., Yamamoto, K., Urabe, I., and Okada, H. (1989) Stability-increasing mutants of glucose dehydrogenase. *FEBS Lett.* **253**, 113–116
55. Kuraulis, P.J. (1991) MOLSCRIPT: a program to produce both detailed and schematic plots of proteins. *J. Appl. Crystallogr.* **23**, 946–950
56. Esnousf, B.M. (1997) An extensively modified version of MOLSCRIPT that includes greatly enhanced coloring capabilities. *J. Mol. Graph.* **15**, 138
57. Merritt, E.A. and Bacon, D.J. (1997) Raster3D: photo-realistic molecular graphics in *Methods in Enzymology* Vol. 277, pp. 505–424, Academic Press, New York